Constructing the fragment size distribution of a bench blasting round, using the new Swebrec function

Finn Ouchterlony[1], Mats Olsson[1], Ulf Nyberg[1], Peter Andersson[1] and Lennart Gustavsson[2]

Abstract

The blasting at the Vändle aggregate quarry has been investigated in order to predict the effect of the specific charge on fragmentation and to assess the contribution of blasting and primary crushing to the -32 mm fines. Two 25000 ton blasts divided into halves were monitored. Each half had an expanded or a shrunken pattern in order to lower or raise the specific charge. A normal round uses Ø90 mm drill-holes on a 3·4 m pattern with a gassed bulk emulsion blend with 20-25 % of AN prills. The test rounds lay directly behind each other, with a shrunken pattern behind an expanded one and vice versa to minimize the influence of geology.

From the muck piles, four test piles of about 500 tons were extracted and photographed for image processing. About a quarter of each was sieved in four steps and fines samples taken. The material was replaced and the whole pile fed to the primary crusher while measuring the effect and the fines produced. Crushability and grindability data were measured.

All lab samples and crushing test samples follow the new Swebrec distribution extremely well. The fragmentation size distribution of the muck piles is constructed using the sieving data and the lab samples, conforming to the Swebrec function. Image analysis gives a fragmentation curve with a distinctly different character. Of the total of 28 % of -32 mm fines after primary crushing, blasting and crushing contribute about half each.

Based on these data a set of design curves are constructed that allow the prediction of how any given fraction changes when the specific charge in the round is changed.

1. INTRODUCTION

Recently a large amount of evidence has been found, which shows that the fragmentation of blasted and crushed rock follows a new cumulative size distribution, the Swebrec function

$$P(x) = 1/\{1+[\ln(x_{max}/x)/\ln(x_{max}/x_{50})]^{b}\} \quad \text{where } 0 < x \le x_{max}. \quad (1)$$

See Ouchterlony (2005a). Hundreds of sieved piles of rock support this finding. The Swebrec function differs from previously used fragment size distributions such as the Rosin-Rammler in the Kuz-Ram and CZM models (Cunningham, 1987; Kanchibotla, Valery & Morrel, 1999) in that it has a finite upper fragment size xmax and a very different behaviour in the fines region.

Apart from x_{max} the new function has two parameters; x_{50}, the average or median fragment size, and a curve undulation parameter b. One doesn't normally expect a relationship between these parameters but the slope values s_{50} at x_{50} suggest that for full size blasts

$$b \approx 0.5 \cdot x_{50}^{0.25} \cdot \ln(x_{max}/x_{50}) \text{ when } x_{50} \text{ is given in mm.} \quad (2)$$

See Ouchterlony (2005b). It is possible to relate b to the uniformity index n of the Kuz-Ram model. Thus, if one retains the prediction equation for x_{50} in the Kuz-Ram and CZM models, then equation 2 could replace the prediction equation for n. Still a good prediction equation for x_{max} remains to be established.

One advantage of the Swebrec function is its wide range of applicability, usually 2 orders of magnitude in fragment size or more. For the bench blasting in the Bårarp quarry e.g. the range was 0.5-500 mm (Moser et al., 2003). This means that the fines part of the size distribution carries information about the coarse part and vice versa (Ouchterlony, 2005a-b). We may thus expect to obtain good estimates of fragment size distributions for muck piles based on a combination of limited data such as i) sieved laboratory samples, ii) partial sieving of test piles, even grizzly data, iii) visual observations of boulders and iv) image analysis values for e.g. x_{50} and x_{80}.

Such techniques have been used in MinBaS project 1.22 *Optimal fragmentation in quarries*, where field work was done at Swerock AB's granite aggregate quarry at Vändle during 2004 (Ouchterlony et al., 2005). This project was a follow up of a state-of-the-art review and had the overall goal of delivering a description of how the blasting in the quarry could be changed so that the desired feed into a primary crusher could be obtained.

The project was also expected to answer questions like:

- Does the real blasted fragmentation at Vändle look like curve no. 63 plus more fines?
- How good is digital image analysis at determining the fragmentation of a blasting round?
- Is the fines fraction of the primary crusher's product much larger than the blasted value?
- What are the respective contributions of blasting and crushing to the road base fraction?
- How do you blast in different rock materials to obtain the desired fragmentation?

2. EXPERIMENTAL CONDITIONS

2.1. Quarry and blasting practice

Swerock AB's Vändle operation lies 15 km South-West of Västerås in Middle Sweden and it quarries a fine to medium

[1] *Swedish Blasting Research Centre, Swebrec at LTU, PO Box 47047, SE-10047 Stockholm, Sweden*

[2] *Aros Grusförädling, PO Box 1106, SE-72128 Västerås, Sweden*

grained, red to reddish grey granite. The mineral contents are typically 35 % quartz, 30-35 % potassium feldspar, 25-30 % plagioclase and 3-5 % biotite plus traces of chlorite and epidote. Other typical data are density 2640 kg/m3, brittleness index 46.8, flatness 1.33 and a grinding index of 2.0-2.6. The joint system in the quarry strikes mainly N-S, with a slight offset to the west. The rock surface is undulating, overlain by till and locally weathered to a depth of 5-8 m with joint infilling of chlorite and calcite.

The quarry layout is mainly E-W with the crushing plant and two bitumen plants in the Eastern part and the workings in the Western and North-West parts. The bench height is usually 11-12 m. The drilling is made with a Tamrock Ranger 700 rig equipped with a Tamrock HL710 hydraulic drill, a Sandvik R51 drill string with Ø89 mm Retrac bits. The rounds normally have 4-5 rows of 20-25 holes on a burden x spacing pattern of 3 x 4 m and a size of 25-40 000 ton. The annual production is about 500 000 ton, of which the road base fraction makes up 20 %.

The holes are drilled at the angle 5:1 with 1.5 m of sub-drill. They are charged with Titan 6075 from Dyno Nobel, a hot gassed site mixed emulsion with 25 % of AN added. The explosive rises 2-3 m in the hole within minutes. Normally 1.5-2 m is left uncharged and filled with 4-8 mm gravel. The targeted specific charge is q = 0.5 kg/m^3. The Nonel Unidet initiation system is used, with a 42 ms in-row delay and a 42 ms (row 1-2) or 67 ms between rows delay. The initiation sequence is of V-type.

The rounds may contain a maximum of 4 % oversize. The remaining material is fed into a rotary jaw crusher, Svedala Arbrå R 120 with an opening of 800 mm and a CSS of 150-160 mm. The road base fraction, basically 0-32 mm, is screened off directly afterwards. To keep this material within the limits given by ATB Väg 2002 (SNRA, 2001), the mesh size of the screens are sometimes changed from the normal 35 mm opening.

2.2. Test lay-out and procedure principles

The tests were conducted in the NW corner of the quarry and planned so as to have i) the maximum difference in fragmentation, ii) a minimal influence on production and iii) a minimal influence of geological variations.

Fragmentation is influenced mainly by the specific charge, which for given production conditions should be the easiest to change by changing the blast hole pattern. The limits were given by achieving a sufficient toe breakage and avoiding flyrock that could damage the bitumen plants. This allowed the use of two patterns, an expanded one of 3.2x4.25 m, which gives q = 0.44 kg/m^3 and a shrunken one of 2.75x3.75 m, which gives q = 0.57 kg/m^3. The change from the nominal value is around ±13 %.

The gauge of a bit wears from Ø90 mm to Ø82 mm before it is discarded after about 600 m of drilling (40-50 holes). To minimise the variations in specific charge that this incurs, it was decided to use 10 new bits for each round instead of the normal 2-3.

It was decided to monitor two production rounds in detail. As the 4 row rounds are about 12 m deep and 80 m wide, the rounds were placed behind each other to minimise geological effects. Each round was divided in two; one half had the higher, the other the lower specific charge. Hereby the crusher production interference was minimised. The halves and corresponding test piles have been denoted 1-L (low q) and 1-H (high q) and 2-H and 2-L respectively. The same V-type initiation pattern was used in both halves.

To get a further handle on geological variations along the face, sub-round 2-H was placed behind 1-L and 2-L behind 1-H. The resulting packet, shown in Figure 1, has a constant depth and thus left the face geometry after the testing unchanged. These principles in essence follow the "matched pair" technique recommended by Brent and Noy (2005).

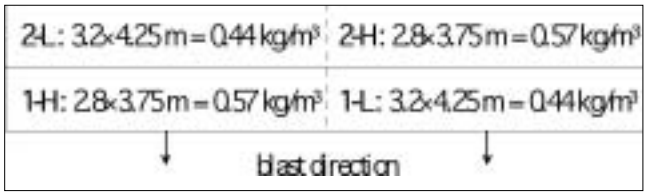

Figure 1: Layout principles of test rounds.

The test rounds contained 25-30 000 ton or around 10000 m^3, each part 5 000 m^3. It was planned that every 25th bucket from the backhoe would be loaded into a dumper and put aside, building four test piles of about 400 ton. Each of these piles would then be flattened to a 15x15 m bed of 1 m height and each pile photographed with a digital camera in order to evaluate the fragmentation with Split (Kemeny et al., 1999).

The sieving procedure would consist of taking about 100 tons from each pile and running them over two grizzlies (250 and 150 mm spacing) and then through a PowerGrid 800 screening plant, first with a 100 mm square mesh screen and then with a 40 mm screen, see Figure 2. All fractions were to be loaded onto trucks and weighed on the quarry's product scale, which has a 20 kg accuracy. From the 0-100 mm fractions and then from the 0-40 mm fractions, samples were to be taken for lab sieving and crushing and grinding tests.

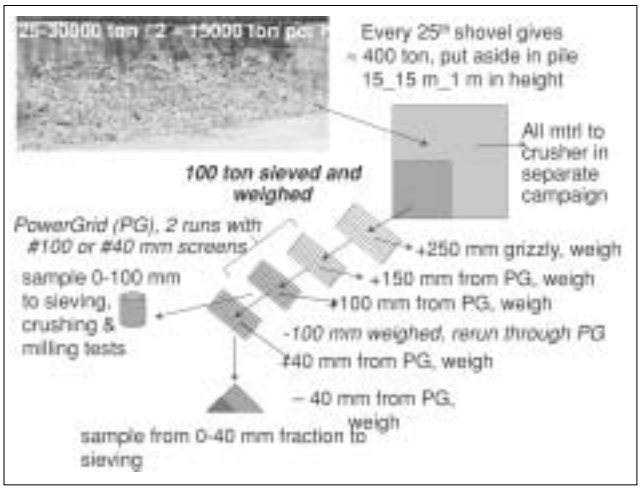

Figure 2: Principles of sieving campaign.

The sieved material would finally be replaced and the whole test piles run through the crusher, while measuring the power required for crushing each pile. The piles were to be weighed by the product belt scale before the road-bed fraction was sieved off and weighed. Lab samples were to be taken from the road-bed fraction for lab sieving. See Figure 3.

3. FIELD CAMPAIGN

3.1. Drilling and charging

The drill rig was equipped with TIM instrumentation, which allows the setting of hole direction, hole depth and penetration rate. The drill hole diameters were sampled with gauges. After drilling, the hole depths were sounded, the collaring positions were measured with Transtronic equipment and the bench face was measured using the QuarryMeter handheld laser

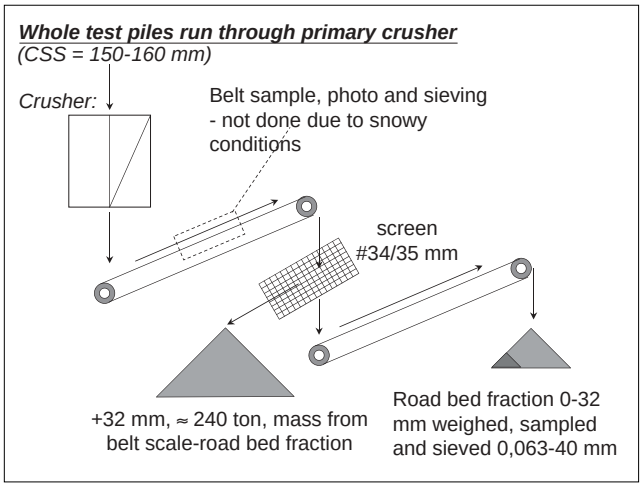

Figure 3: Principles of crushing campaign.

instrumentation. The drill pattern of Round 1 is shown in Figure 4. The measurement statistics are given in Table 1. It may be seen that the burden and spacing data lie within 10 cm of the planned values, except the burden of round 2-L, which on average is about 25 cm too large.

Table 1: Summary of round data and drilling statistics (mean ± standard deviation)

Round:	1-L	1-H	2-H	2-L
Bench height (m)	12.2	11.4	12.7	10.8
Hole diameter (mm)	90	90	90	90
Hole angle (º)	10	10	10	10
No. of rows	4	4	4	4
Hole no. in 1st row	1-8	9-19	1-10	11-21
No. of holes	31	44	40	43
Hole depth (m)	13.7±0.8	12.7±0.9	14.2±1.1	12.4±0.8
Sub drilling (m)	1.3	1.1	1.2	1.4
Burden (m)	3.18±0.07	2.86±0.11	2.89	3.46
Spacing (m)	4.27±0.07	3.80±0.15	3.71	4.17
Volume of round (m^3)	4638	4956	4902	6233

Note: L = low specific charge and H = high specific charge.

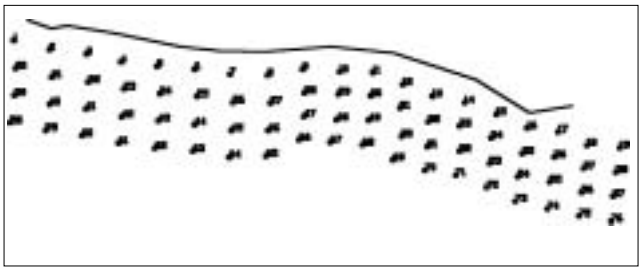

Figure 4: Measured collaring positions of drill holes in Round 1.

The bulk truck allows for individual logging of explosive charge per hole (Nilsson & Perlid, 2004). The manufacturer's data for Titan 6075 are given in Table 2. The charging aimed at giving a constant uncharged part. It went mostly as planned. Some holes were water logged but the explosive charging usually displaces this water. Two holes couldn't be sounded due to clogging but they could be charged as planned. The statistics of the charging data are given in Table 3.

Table 2: Manufacturer's data for explosive Titan 6075

Density (kg/m^3)	1200
Weight strength rel. to ANFO (%)	85
Volume strength rel. to ANFO (%)	113
Explosion energy (MJ/kg)	3.34
Velocity of detonation, VOD (m/s)	4300
Gas volume (litre/kg)	950
Percentage AN-prills (%)	25

Table 3: Summary of charging data and statistics

Round:	1-L	1-H	2-H	2-L
Titan 6075 total (kg)	2650	3417	3711	3304
Charge (kg/hål)	86±7	78±8	93±12	77±7
Uncharged (m)	2.1±0.4	2.2±0.4	2.2±0.8	2.1±0.8
- fraction of bench	0.176	0.194	0.172	0.191
Charge length (m)	11.5±1.0	10.4±1.0	12.0±1.3	10.3±1.0
Charge conc. (kg/m)	7.4±0.3	7.4±0.4	7.7±0.4	7.5±0.4
Density (kg/m^3)	1170±50	1180±70	1230±60	1180±60
Specific charge (kg/m^3)				
- planned	0.44	0.57	0.57	0.44
- per hole	0.52	0.63	0.68	0.49
- per round volume	0.57	0.69	0.76	0.53

The table shows that the calculated charge concentration of Titan 6075 is quite even, 7.4-7.5 kg/m, except for round 2-H. This corresponds to a density of 1170-1180 kg/m^3 compared with the nominal value 1200 kg/m^3. Individual holes had apparent charge concentrations as low as 5.9 kg/m, probably due to a mixing with water and drill cuttings, and as high as 9.3 kg/m, probably due to leakage into fractures.

The resulting specific charge values became higher than planned, probably due to the use of nearly new drill bits, which hadn't been accounted for in the charge calculations.

3.2. Blasting and loading

Each half-round was initiated in the middle, with a 25 ms delay between. A small amount of muck was present in front of the face of round 1, none in front of round 2. The VOD was measured, using MREL's Minitrap equipment, in holes 15-19 in row 1 of round 1-H and holes 1-5 in row 1 of round 2-H. The rounds were videotaped and their function appears to have been satisfactory. Round 1 was blasted on June 24th and round 2 on November 3rd, 2004.

Table 4: Measured VOD-data in m/s

	Round 1-H			Round 2-H	
Hole no.	Bottom	Top	Hole no.	Bottom	Top
15	4743	4517	1	4295	4390
16	4427	4388	2	5091	4267
17	5146	4859	3	4688	3219
18	5079	4544	4	5049	4960
19	5276	4197	5	4786	
mean	4934	4501		4782	4209
std dev.	345	243		321	726

A good VOD curve is shown in Figure 5 and the measured values are given in Table 4. The VOD curves from round 1 were all smoother than the curves of round 2, which all had some irregularities. The VOD statistics became 4718±362 m/s for round 1-H and for 2-H excluding hole 3 they became 4771±275 m/s. While higher than the nominal 4300 m/s the explosive appears to have worked well but the irregularities from round 2-H detract from the overall function of round 2.

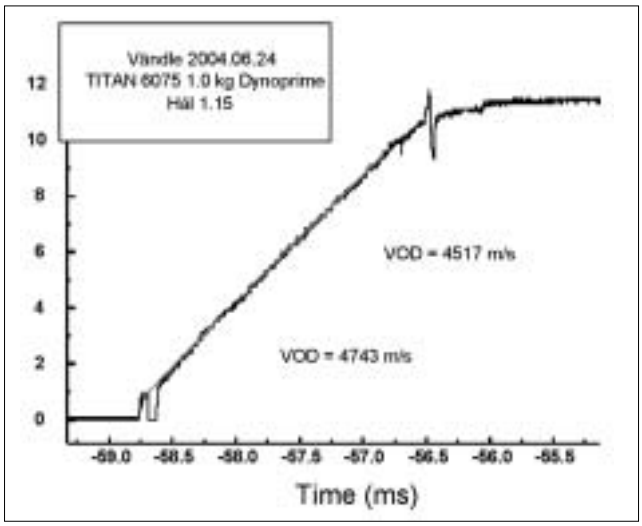

Figure 5: VOD-curve for hole 15 in Round 1-H.

Photos of the muck piles are shown in Figures 6a-b. The trough in the middle contains material from both halves and a conscious effort was made not to include any mixed material from the troughs in the test piles.

Figure 6a: Round 1 after blasting, on the left Round 1-H, on the right Round 1-L.

Figure 6b: Round 2 after blasting, on the left Round 2-L, on the right Round 2-H.

Round 1 was blasted on June 24th but an unforeseen delay in the loading of round 1, threatened to push the blasting and loading of round 2 into winter conditions. Thus only the loading of round 1-L went as planned (June 28th to Sep 27th). Round 1-H (Sep 28th to Oct 25th) was speeded up by the backhoe loading directly into a mobile crusher. Round 2 was blasted on Nov 3rd. Rounds 2-H and 2-L were mucked out in parallel during Nov 3rd to 17th, a backhoe and mobile crusher pair used on each. This speeded up the loading considerably but made the building of the test piles more uncertain as the dumpers weren't directly in the production cycle.

The main part of the sieving and crushing work on the test piles was done during the week of Nov 15th-19th, at the end of which a snow storm complicated the work in the quarry. The snow hardly influenced the results for round 1, which was treated first, but tendencies for freeze caking influenced the results for round 2. Figure 7 shows the test piles on the quarry floor before the photography and sieving started.

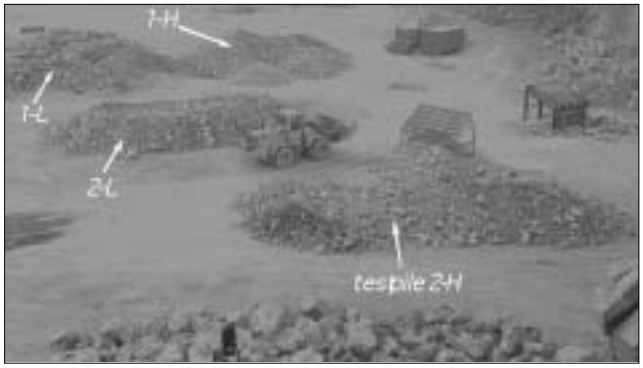

Figure 7: Test piles on quarry floor before sieving campaign.

4. FRAGMENT SIZE DISTRIBUTIONS

4.1. Sieving data

The sieving procedure; 250 and 150 mm grizzlies, 100 and 40 mm square mesh screens, gave the following data in Table 5. A first impression is that the average fragment size lies around 150 mm and that the fragmentation in pile 1-H is finer than in pile 1-L. The results for piles 2-L and 2-H are quite similar and the reasons for this are discussed at some length (Ouchterlony et al., 2005). The result is that the pile 2 results were judged to be less representative of the round 2 fragmentation and less credible than the round 1 results.

Table 6 shows the results of the crushing campaign, both the total amounts of each pile and the road bed fractions screened off with a 35 mm mesh screen. These fractions contain at least 98 % of -32 mm material.

A comparison of Tables 5 and 6 shows that the road bed fraction in the crusher product on average is nearly 28%

Table 5: Weighed fractions from sieving of test piles and cumulative passing, excl. boulders

Round:	1-L		1-H		2-H		2-L	
Fraction (mm)	(ton)	(%)	(ton)	(%)	(ton)	(%)	(ton)	(%)
+250	26.60	100.0	19.20	100.0	27.18	100.0	24.12	100.0
150-250	25.42	74.5	31.94	84.2	30.94	73.2	29.22	75.2
100-150	19.28	50.2	25.16	58.0	18.74	42.7	18.58	45.3
40-100	16.32	31.7	23.02	37.4	13.72	24.2	15.46	26.3
0- 40	16.86	16.1	22.58	18.5	10.80	10.7	10.12	10.5
Total sieved (ton)	**104.48**		**121.90**		**101.38**		**97.50**	

Table 6: Weighed fractions from sieving of crushed test piles

Round:	1-L		1-H		2-H		2-L		Alla
Fraction (mm)	(ton)	(%)	(ton)	(%)	(ton)	(%)	(ton)	(%)	(ton)
+35	506.3	72.6	401.6	70.5	244.7	73.6	316.8	72.4	72.1
-35	191.2	27.4	168.0	29.5	87.9	26.4	121.0	27.6	27.9
Total	**697.5**	**100.0**	**569.6**	**100.0**	**332.6**	**100.0**	**437.8**	**100.0**	**100.0**

and that the blasting contributes almost exactly half or 14.2 % of this material.

The lab samples were sieved down to 0.063 mm by an accredited NCC road laboratory. Figures 8a-c show the cumulative fragment size distributions. The samples from the 0-100 mm fraction in Figure 8a show that the samples from pile 1 show a high degree of reproducibility as do the samples from pile 2 but that there is a slight difference between the two rounds. The same observations are basically valid for the 0-40 mm samples in Figure 8b. Taking the value for the 22.4 mm mesh as a reference, the curves from 0-40 mm samples lie at most 2-3 % below the curves for the 0-100 samples and the average curves well within 2 % of each other.

There is no systematic difference between the curves for the crushed road bed fractions from the different piles in Figure 8c. A comparison of Figures 8b and c show however that the blasted samples contain more fines, on average at most 7 % for 8 mm fragments.

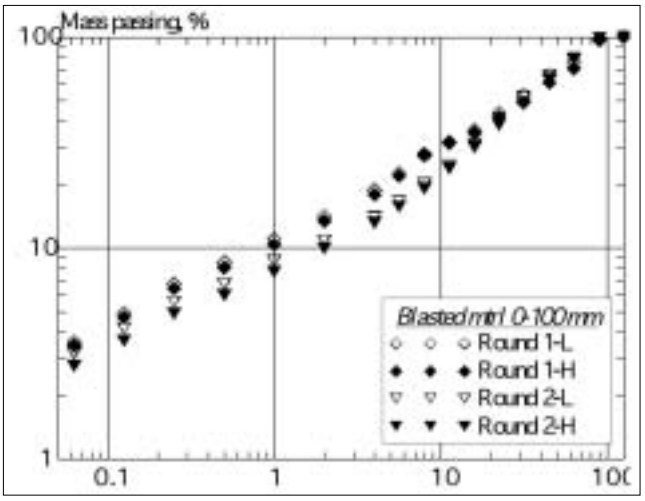

Figure 8a: Sieving curves for 0-100 mm fraction samples from test piles.

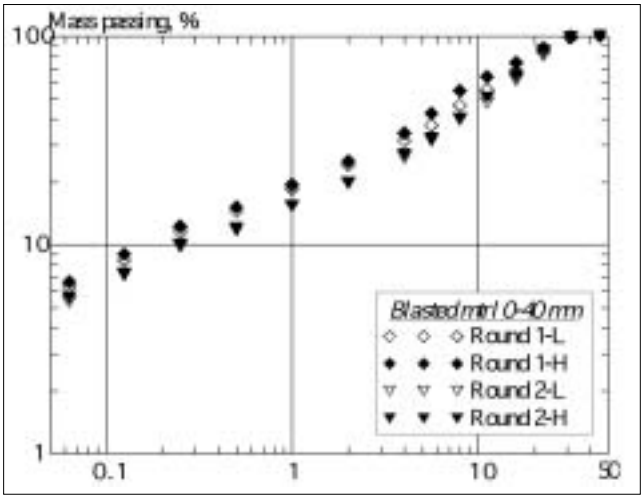

Figure 8b: Sieving curves for 0-40 mm fraction samples from test piles.

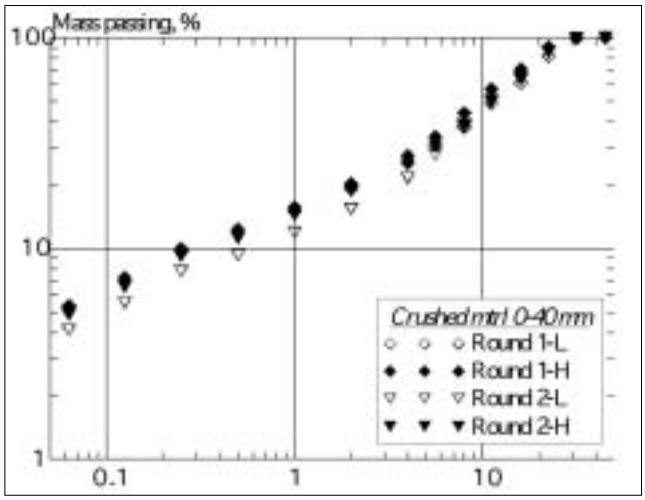

Figure 8c: Sieving curves for 0-40 mm fraction samples from crushed material.

A curve fitting to the lab sample data using the Swebrec function of Equation 1 gives an almost perfect fit with r^2 values of 0.997 or better over the intervals 0.25-31.5 and 0.25-90 mm respectively. Furthermore the residuals are basically stochastic. An example is shown in Figure 9 and curve fit statistics are given in Table 7.

The oversize was estimated both by boulder counting and by using Split, see Figure 10. The estimated amount was low, within 1.2-1.9 % of the rounds. The average boulder size was about 0.6 m but the oversize piles contained fragments from about 0.25 m and up.

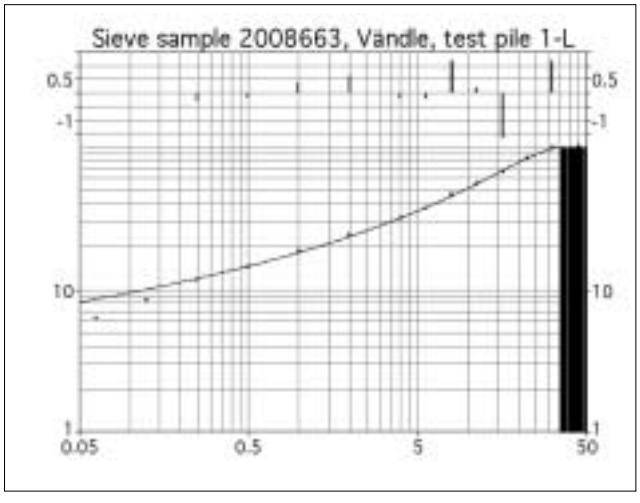

Figure 9: Swebrec function fit to sieving data for sample from 0-40 mm fraction, Round 1-L.

Table 7: Swebrec function parameter values for lab sample sieving data							
Sample and origin	**X_{50} (mm)**	**X_{max} (mm)**	**b**	**Range (mm)**	**r^2**	**S_{50} (1/mm)**	**$S_{50} \cdot X_{50}^{0.75}$ (1/mm0.25)**
0-100 mm from round							
1-L	27.7	135	1.845	0.25-90	0.997	0.011	0.127
1-H	30.0	158	1.905	0.25-90	0.991	0.010	0.122
2-H	33.1	108	1.817	0.25-90	1.000	0.012	0.160
2-L	31.4	113	1.838	0.25-90	0.998	0.011	0.152
0-40 mm from round							
1-L	9.5	34.8	1.494	0.25-31.5	0.999	0.030	0.164
1-H	7.4	37.1	1.764	0.25-31.5	0.998	0.037	0.166
2-H	11.0	31.5	1.459	0.25-31.5	1.000	0.032	0.190
2-L	11.8	32.6	1.411	0.25-31.5	1.000	0.029	0.187
0-35 mm from crusher							
1-L	11.8	31.5	1.473	0.25-31.5	0.999	0.032	0.202
1-H	12.0	31.5	1.387	0.25-31.5	1.000	0.030	0.193
2-H	11.9	31.5	1.593	0.25-31.5	0.999	0.034	0.221
2-L	9.6	31.5	1.612	0.25-31.5	0.999	0.035	0.193

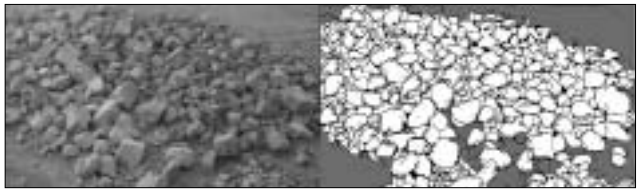

Figure 10: Photo of boulder pile from Round 2-H and retouched Split delineation.

4.2. Construction of complete sieving curves

The construction of the complete sieving curves for the test piles was accomplished as follows:

1) The Swebrec function is relatively linear within the range of 10-60 % passing and the cumulative sieving data for 40 and 100 mm mesh sizes lie well within this range. They are the "fixed points" of the construction. Data points for 45, 63 and 90 mm mesh sizes are taken from a straight line interpolation and the 125 mm point taken as an extrapolated value on the same line.
2) The lab samples from the 0-100 mm fractions are assumed to be relatively uninfluenced by the original sampling for the -40 mm material. As 40 mm is missing in the lab screen series, the 40 mm data point was interpolated from the 31.5 and 45 mm data points. An example is pile 1-L where the cumulative percentages 52.6 and 66.0 % give the value 61.03 % at 40 mm. The sieved 40 mm value in step 1) above is 16.1 %. The lab sample data for all smaller screen sizes are thus scaled by the factor 16.1/61.0 ≈ 0.264. This makes the lab sample data a continuation of the interpolation line into the fines region. The continuation is expected to be relatively, if not exactly smooth.
3) A grizzly with a given gap lets through larger fragments than a square mesh with the same dimensions. To account for this the grizzly gap values 250 and 150 mm have been multiplied with a flakiness factor. A lower limit is given by the interpolation line of step 1). Here we let the flakiness factor be determined by that curve fit, which gives the highest r^2 value. I.e. a flakiness factor was chosen, the curve fit program TableCurve2D run and a new flakiness value chosen until the r^2 maximum was found. This value turns out to be 1.10 or 1.15. We have chosen the flakiness value 1.10 here.
4) To construct the fragmentation curve of the test piles we do not need to know the amount of oversize, which is about 1-2 %. Furthermore, the lower cut off size in the boulder piles was not sharp but it started at about 0.25 m. A visual judgement gave 0.4-0.5 m as a reasonable largest fragment size in the test piles. For the construction of the fragmentation curves we have chosen 400 mm as a representative grizzly gap, which is then multiplied by the flakiness factor of step 3). This data point has been used in the curve fitting.
5) Taking the uncertainties involved in the construction of the test piles and their representativity, it doesn't matter much if the test piles represent 98 or 99 % of the muck pile volumes. In the following it is assumed that the test piles represent 100 % of the muck pile material. With a better monitoring of the oversize material, it could and should of course be included in the construction procedure.

A set of numerical values for pile 1-L is given in Table 8 and the constructed fragmentation curve in Figures 11 a-b. The best Rosin-Rammler distribution around the fixed points is shown as dashed lines. It doesn't fit well either in the fines or coarse material ranges. A weighting to improve the fit in the coarse range would worsen it in the fines range.

The parameters for Swebrec curve fits are given in Table 9. The difference in fragmentation between rounds 1 and 2 is clear. The result that x_{50} for round 2-H is coarser than for round 2-L is suspect of course. The values of the slope s_{50} at x_{50} and of the composite parameter $s_{50} \cdot x_{50}^{0.75}$ are given too. The expected value for the latter is about 0.12 (Ouchterlony, 2005b). The values for round 1 are nearly spot on but those for round 2 a bit higher.

4.3. Comparison with image analysis results and rock material curves

The images of the test piles were taken from a skylift above the piles (top images) or from the ground (side images) using basket balls as sizing objects. Figure 12 shows the approximate position of each image for pile 1-L. Those marked with an asterisk were processed further by Greg Potts, who has experience with the Split system (Potts and Ouchterlony, 2005). Due to the rush caused by the impending snow storm, piles 2-L and 2-H were not complete when the images were taken.

Split DeskTop was used in the *auto delineation* mode with a *fines factor* ff = 50 %. Two important error sources are the program's tendency to section large blocks and fuse small

Table 8: Data behind and steps in construction of complete sieving curve for test pile 1-L

Type of data:	Mesh data	Sample 0-100 mm	Weighed amount	Calculated cumulative	Splice 40 mm	Final curve
Screening type	**Size mm**	**Passing %**	**Fraction ton**	**Passing %**	**Passing %**	**Passing %**
Grizzly	440[2]		26.60	100.00		100.00
Grizzly	275[2]		25.42	74.54		74.54
Grizzly	165[2]		19.28	50.21		50.21
Extrapolated	125			38.85		38.85
PowerGrid	100	100.00	16.32	31.76		31.76
Interpolated	90	97.65		29.15	(25.82)	29.15
Interpolated	63	75.96		22.12	(20.08)	22.12
Interpolated	45	66.00		17.44	(17.45)	17.44
PowerGrid	*40*	*61.03[1]*	*16.86*	*16.14*	*16.14*	*16.14*
Lab sample	31.5	52.59			13.90	13.90
Lab sample	22.4	43.81			11.58	11.58
Lab sample	16	36.13			9.55	9.55
Lab sample	11.2	31.50			8.33	8.33
Lab sample	8	27.42			7.25	7.25
Lab sample	5.6	22.57			5.97	5.97
Lab sample	4	18.89			4.99	4.99
Lab sample	2	14.18			3.75	3.75
Lab sample	1	10.99			2.91	2.91
Lab sample	0.5	8.55			2.26	2.26
Lab sample	0.25	6.74			1.78	1.78
Lab sample	0.125	4.92			1.30	1.30
Lab sample	0.063	3.59			0.95	
0.95						
Total (ton)			**104.48**			

Note 1: Interpolated point from lab sample data at 31.5 and 45 mm.
2: Actual grizzly spacing times flakiness factor, in this case 1.10.

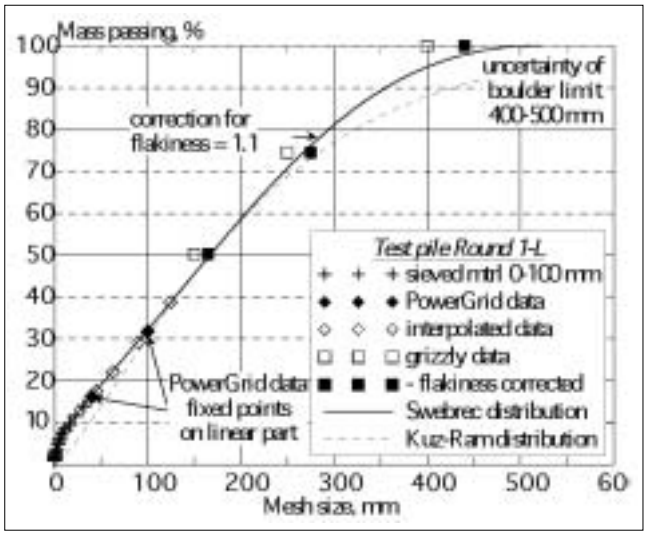

Figure 11a: Constructed sieving curve for test pile from Round 1-L, linear scales.

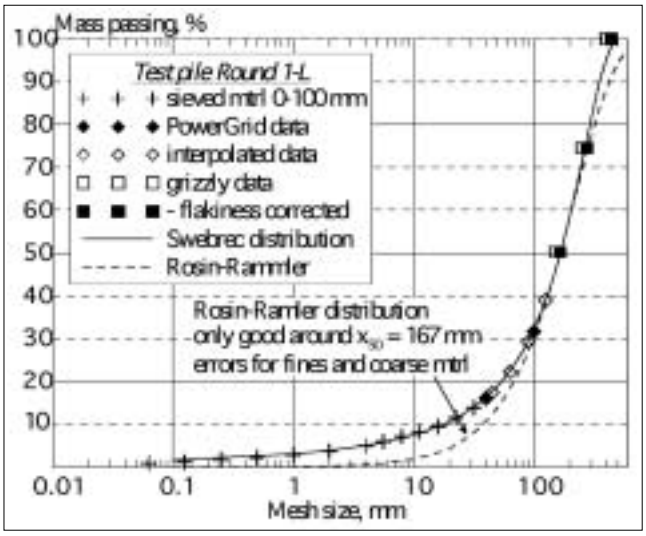

Figure 11b: Constructed sieving curve for test pile from Round 1-L, log-lin scales.

Table 9: Swebrec function parameter values for constructed complete sieving curves

Test pile	X_{50} (mm)	X_{max} (mm)	b	r^2	S_{50} (1/mm)	$S_{50} \cdot X_{50}^{0.75}$ (1/mm0.25)
1-L	167	522	2.016	0.9993	0.00265	0.123
1-H	141	450	1.965	0.9989	0.00301	0.123
2-H	190	524	2.300	0.9997	0.00299	0.153
2-L	180	550	2.464	0.9997	0.00306	0.151

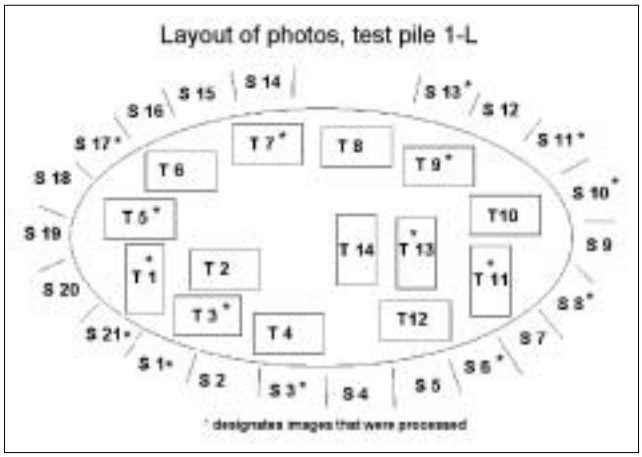

Figure 12: Placing of top and side images on test pile 1-L.

ones. Therefore 10 to 25 minutes per image were spent touching up the block boundaries, basically obliterating the effect of specific parameter settings. Figure 13 shows an example.

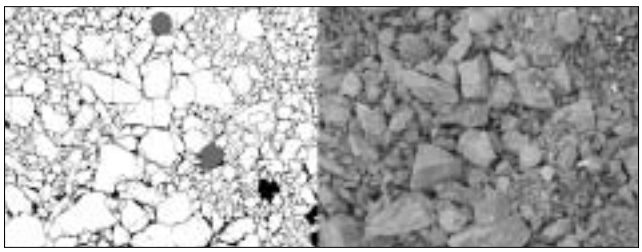

Figure 13: Image Top 1 from test pile 1-H; retouched Split delineation and digital photo.

The lowest *fines cut-off* in the images lay in the range 10-20 mm but usually it lay above 50 mm. Different ways of treating the data were tried and the following conclusions were reached

- If the *fines cut-off* is expressed in pixels, it may be used to judge the optimal resolution of the images.
- It is normally not an advantage to take several image of material that fits in a single image.
- Taking several images is an advantaged if their scales are different.
- It is proper procedure to use the maximum resolution when taking the image and then reduce to the optimal value before the analysis. If the fines are judged to be underrepresented, images with a higher resolution could be selected for analysis.

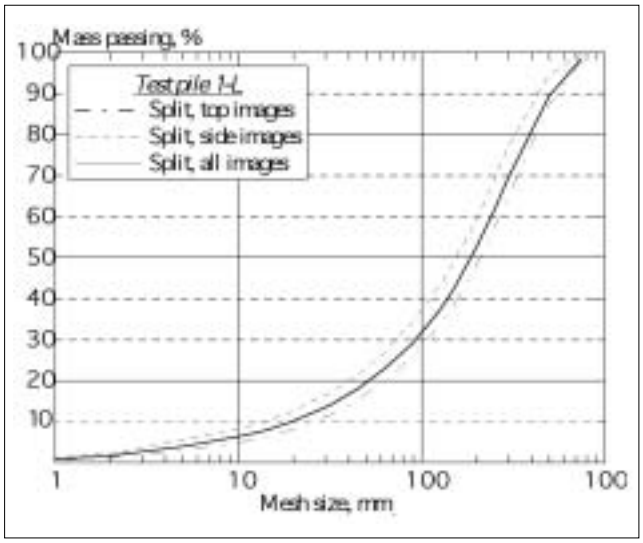

Figure 14: Sieving curve from Split analysis of test pile 1-L images.

Of 12 top images for pile 1-L, 7 were analysed in detail and 7 of the 21 side images. The fragmentation correlation between neighbouring top and side images was not very high. The fragmentation curves for pile 1-L are shown in Figure 14. The full curve marked “all images” is a result of Split’s merging algorithm. This merging is not a pure averaging as the “all image” curve for round 2-H for the most part lay below the “top images” and “side images” curves.

The statistics for the fragmentation data obtained with Split DeskTop are given in Table 10.

The table shows that proper size range of the method is “cut-off” to “top-size” or roughly one order of magnitude in fragment size. This means that more than half of the curves in logarithmic Figure 14 consists of extrapolated data, which is basically of Rosin-Rammler type. The high cut-off values are the averages for the individual images; in a few cases the cut-off value is higher than the resulting x_{50} value. The data in Table 10 basically support the conclusions drawn for the constructed sieving curves in Table 9.

Figures 15a-d show the comparison between the constructed sieving curves and the curves from the Split analysis. The Split curves have a different form than the sieving curves. They are skewed, being flatter in the coarse range and steeper in the fines range, thereby predicting more boulders in the test piles. This difference is illustrated in Table 11. We know that the fines parts of the Split curves are definitely wrong; hardly any sieved distribution of blasted rock displays Rosin-Rammler or Gaudin-Schuhman behaviour over a wide range (Ouchterlony, 2005a).

Table 10: Statistics for sieving data from image analysis. All numbers in mm

Test pile	No. of photos	View	X_{20}	X_{50}	X_{80}	Cut-off	Top-size
1-L	7	Top view	66±13	221±50	422±94		
	9	Side view	43±22	158±32	331±87		
	16	All images	53	189	388	85-161	885
1-H	7	Top view	23± 7	131±25	310±58		
		Side view	-	-	-		
	7	All images	28	136	314	65-108	654
2-H	2	Top view	28±18	132±12	313±73		
	6	Side view	38±12	141±20	293±49		
	8	All images	40	145	301	75-131	763
2-L	2	Top view	40±14	149±45	304±85		
	6	Side view	36±18	127±45	259±86		
	8	All images	42	139	297	55- 83	664

Table 11: Comparison of sieving and image analysis data for test pile fragmentation												
Round:	**1-L**			**1-H**			**2-H**			**2-L**		
	sieve	**image**	***diff %***	**sieve**	**image**	***diff %***	**sieve**	**image**	***diff %***	**sieve**	**image**	***diff %***
X_{20} (mm)	54	53	-2	43	28	-35	82	40	-51	77	42	-46
X_{50} (mm)	167	189	13	141	136	-4	190	145	-24	180	139	-23
X_{80} (mm)	294	388	32	254	314	24	301	301	0	291	297	2
X_{max} (mm)	522	885	70	450	654	45	524	763	46	550	664	21

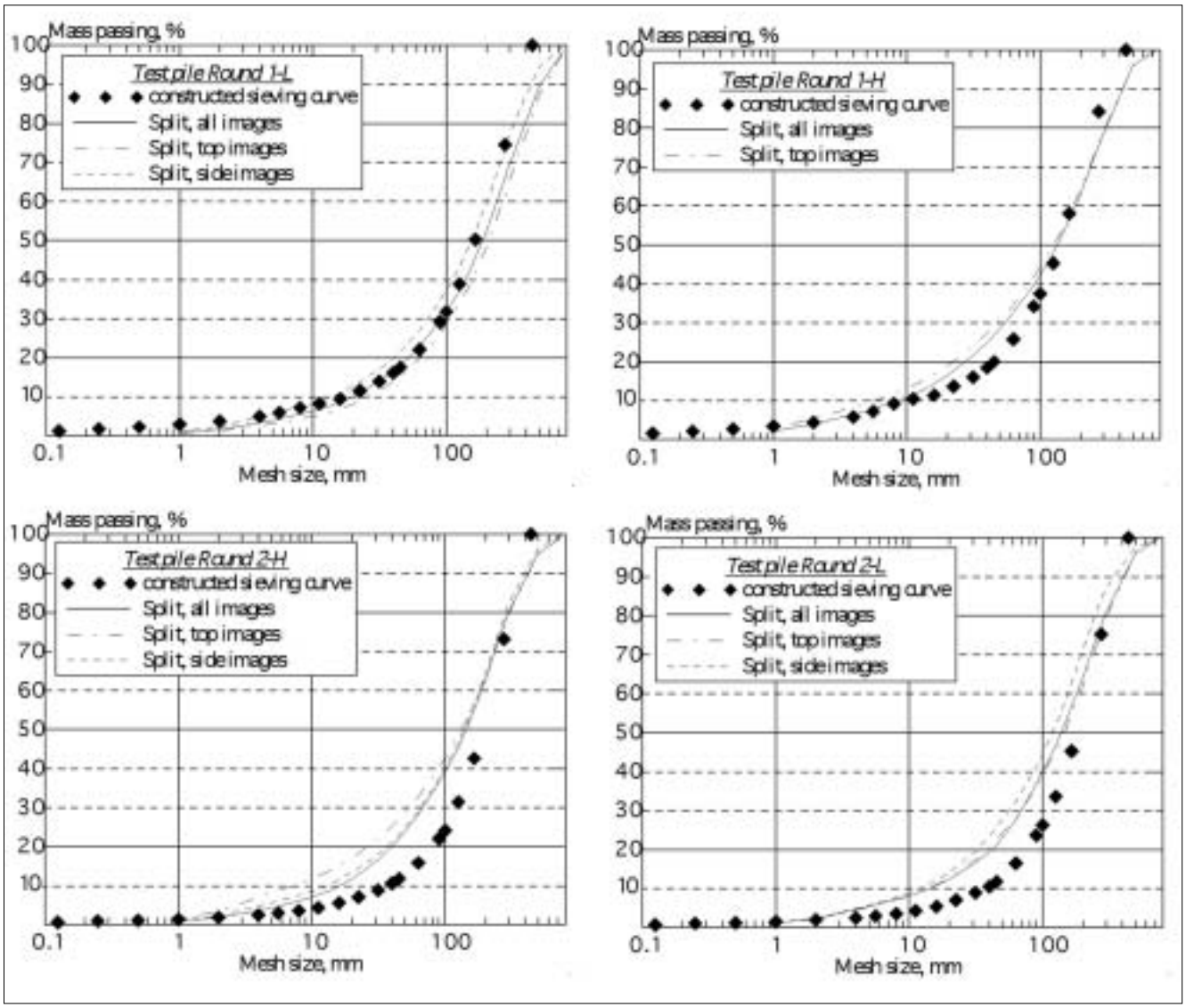

Figures 15a-d: Comparison between sieving curves either determined by image analysis (Split, full curve) or constructed from actual sieving data (diamonds).

For round 1, piles 1-L and 1-H, the x_{50} values are reasonably close but for round 2, the Split values are about 25 % lower. This may have been caused by the piles being incomplete when they were photographed and the tendency for the freeze caking during sieving, rather than being an error associated with the image analysis method as such.

The detailed analysis (Ouchterlony et al., 2005) gave the result however that i) the fragmentation data for round 1 are the most reliable ones and that ii) the sieving data are more reliable than the Split data.

The constructed sieving curves for all test piles are compared with two typical rock material curves used by crusher manufacturers to design crushing plants, curves no. 62 and 63 in Figure 16. The sieving data obviously cluster more around curve no. 62 and they appear to be steeper in the coarse range. Rock material curve no. 62 appears to be a good description of the muck pile fragmentation at Vändle. Interestingly, the whole suite of rock material curves no. 62-66 is expressible in terms of Swebrec functions with $r^2 > 0.995$ (Ouchterlony et al., 2005).

5. BLAST DESIGN CURVES

The most wide spread fragmentation model is the Kuz-Ram (Cunningham, 1987; 2005). The predictions equation for the average fragment size is given by

$$x_{50} = A \cdot Q^{1/6} \cdot (115/s_{ANFO})^{19/30} / q^{0.8}, \quad (3)$$

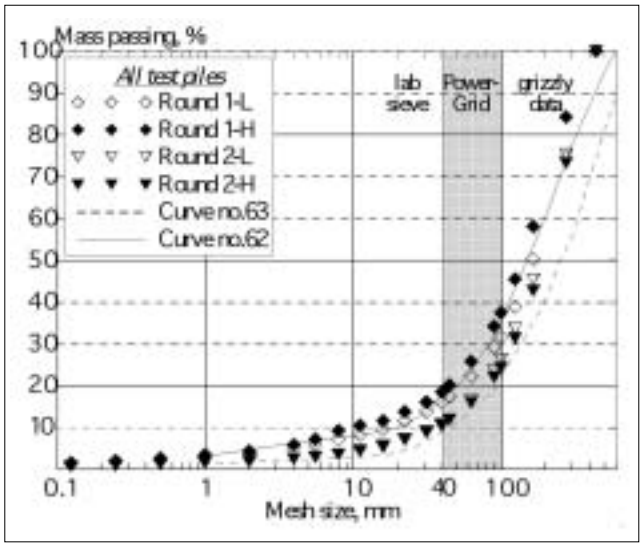

Figure 16: Comparison between sieving data for test piles and rock material curves.

where

x_{50} = median or size of 50 % passing in cm!
Q = charge weight per hole (kg)
q = specific charge (kg/m^3)
s_{ANFO} = explosive's weight strength relative to ANFO (%)

Further the rock mass factor A lies in the range 0.8-21 and it is given by

$$A = 0.06 \cdot (RMD + RDI + HF), \quad (4)$$

where

RMD = Rock mass description = 10 (powdery/friable), JF (if vertical joints) or 50 (massive)
JF = Joint Factor = JPS + JPA = Joint Plane Spacing + Joint Plane Angle
JPS = 10 (average joint spacing S_J < 0.1 m), 20 (0.1 m-oversize x_O) or 50 (> oversize)
JPA = 20 (dip out of face), 30 (strike ⊥ face) or 40 (dip into face)
RDI = Rock density influence = $0.025 \cdot \rho$(kg/m^3) – 50
HF = Hardness factor, based on compressive strength σc(MPa) or Young's modulus E(GPa) = E/3 if E < 50 or σc/5 if E > 50 GPa.

A sensitivity analysis of the A equation shows that for aggregate rock conditions in Sweden, the RDI value is basically constant, the HF value may change somewhat and that the major influence factor is jointing's influence through the RMD term. The individual terms are now somewhat different (Cunningham, 2005).

Table 12: Back calculated rock mass constant A from constructed sieving curves data.

Round:	1-L	1-H	2-H	2-L
X_{50} (mm)	167	141	190	180
q (kg/m^3)	0.52	0.63	0.68	0.49
s_{ANFO} (%)	85	85	85	85
Q (kg/hole)	86	78	93	77
A	3.89	3.89	5.41	4.07

Entering the explosives data from Table 2, the charging data from Table 3 and the x_{50} data from Table 9 into equation 3, the data in Table 12 are obtained. The back calculated rock factor values A' = 3.89 and 4.07 are practically equivalent. The value 5.41 for round 2-H may indicate different rock conditions, rock material or rock mass conditions for the NE corner of our test area.

There are basically no data to support that the rock material of round 2-H was different. The crushing and grinding tests that were made on test samples from the different test piles do not show any significant systematic differences. The simplest interpretation of the available single particle bed crushing data, inter particle bed crushing data, Bond's work index data and ball mill data all point in this direction (Ouchterlony et al., 2005). Thus, if the A-value for pile 2-H represents different rock conditions, then jointing is a possible cause.

Our visual observations do not directly support that the rock in round 2-H is more massive though. Again other explanations have been sought (Ouchterlony et al., 2005) but none have an obvious credibility. Therefore we assign the rock factor A' = 3.9 to the Vändle rock.

The density of the Vändle granite, 2640 kg/m^3 makes RDI = 16. An estimated modulus of 40 GPa makes HF ≈ 13.3. The rock mass has vertical jointing so RMD = JF = JPS+JPA. As the major joints strike relatively perpendicular to the bench face JPA = 20 and by visual inspection the average joint spacing is less than the oversize but larger than 0.1 m. Thus JPS = 30, RMD = 50 and A ≈ 4.76, which is pretty close to the A' value. This shows that the x50 prediction equation could be relatively useful for the Vändle quarry.

Rather than looking for the causes for the difference between A' and A in detail, we introduce the practical correction factor C(A) = A'/A = 3.9/4.76 = 0.82 (Cunningham, 2005). We thus arrive at the following rock corrected mass factor for Vändle

$$A' = 0.05 \cdot (RMD + RDI + HF). \quad (5)$$

Cunningham (2005) also has other correction factors in his new version of the Kuz-Ram model but they are not considered meaningful to introduce here since the experimental basis is yet too small.

In the original version of the model (Kuznetsov, 1973) there are 3 rock classes; A = 7 for medium hard rocks, A = 10 for hard but highly fissured rocks and A = 13 for very hard but weakly fissured rocks. These values may not be directly comparable with our A-values though as there appears to be different definitions of average fragment size (the mean or the median x_{50}) involved (Spathis, 2004).

There are a number of different ways of calculating A. Kanchibotla, Valery and Morrel (1999) have one, Onederra, Esen and Jankovic (2004) a slightly different one. Lilly (1992), who developed the origin of the A-factor, would e.g. have added another 20 points to the RMD value, because the rock mass is blocky, or 1.2 to the A-value. The only effect would be to change the value of the correction factor C(A) though so this line is not pursued here. The detailed data of the jointing is not sufficient to be able to specify which theoretical A formula is the most appropriate one.

Since our aim is to produce blast design curves for Vändle based on the Swebrec distribution, we need more prediction equations, one for b and one for x_{max}. Equation 2 will be used for b but we have no direct basis for the remaining one. A first proposition would be that x_{max} depends on the smallest of the values burden, spacing and joint spacing, i.e. x_{max} is independent of the specific charge. Taking the values above, x_{max} = 500 mm, A' = 3.9,

Table 13: Calculated values of Swebrec parameters for Vändle design curves.							
q (kg/m^3)	0.3	0.4	0.5	0.55	0.6	0.7	0.8
X_{50} (mm)	259	205	172	159	148	131	118
Proposition 1							
x_{max} (mm)	500	500	500	500	500	500	500
b	1.322	1.684	1.934	2.033	2.119	2.263	2.380
Proposition 2							
X_{max} (mm)	710	600	525	500	475	435	405
b	2.025	2.029	2.022	2.033	2.030	2.028	2.033

Q = 83.2 kg/hole and s_{ANFO} = 85 % for Titan 6075 and calculating the curves for a set specific charge values in the range q = 0.3-0.8 kg/m^3 yields the results in Figure 17. The value q = 0.3 kg/m^3 may not achieve a proper toe breakage though. The corresponding b and x50 values are given in Table 13.

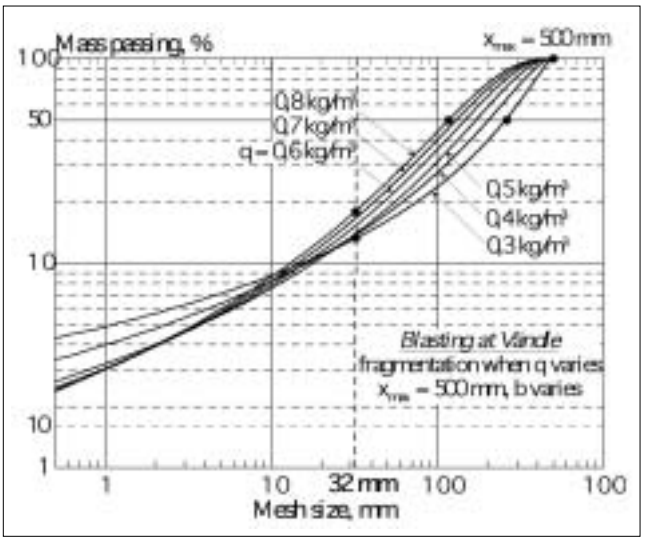

Figure 17: Effect of changing specific charge on fragmentation when xmax is constant.

The figure shows a set of curves which are reasonable around x_{50} but not in the fines range where they cross each other between x = 2.5 and 25 mm. The consequence would be that blasting with a lower specific charge would yield a higher proportion of fines than blasting with a higher one. This is hardly realistic and this probably influences the fragmentation curves in Figure 17 already around the 32 mm point.

As a consequence it is probable that the prediction equation for x_{max} must depend on the specific charge, just as x_{max} in Table 9 is lower for pile 1-H than for pile 1-L. A second proposition could be that it depends on q in such a way as to make b ≈ constant, see Table 13. This corresponds to $x_{max} \approx 500=(0.55/q)^{0.6}$ with x_{max} in mm and q in kg/m^3 of Titan 6075. The resulting set of curves is given in Figure 18.

A third proposition could be that the rock for sufficiently small fragments obeys the "Natural Breakage Characteristic" of that material. The NBC concept (Steiner, 1998) in short means that i) rock, which is crushed or ground in optimal comminution circuits, has fragmentation curves that are the steepest possible, that ii) the fragmentation curves with an increasing comminution are parallel shifted upward in a log-log diagram (not shifted to the left), that iii) when the specific surface (m^2/kg) created during each sub-circuit is plotted versus the comminution

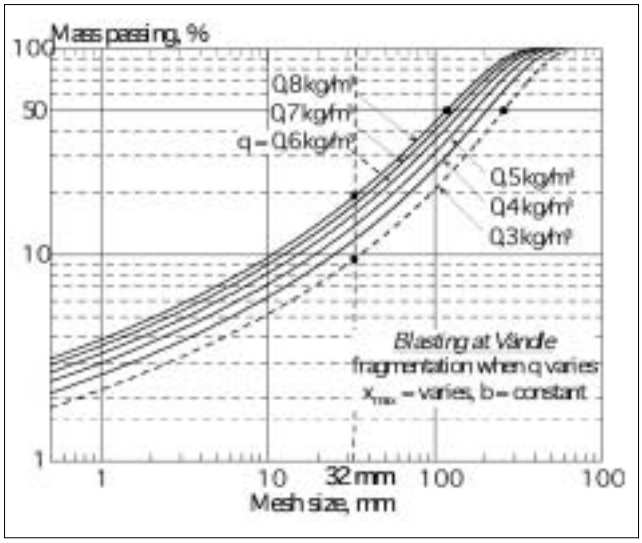

Figure 18: Effect of changing specific charge on fragmentation when b is constant.

energy supplied (J/kg) a reasonably straight line, the "energy register" is obtained and that iv) all real comminution circuits have flatter fragmentation curves and are less energy efficient.

Moser et al. (2000, 2003) have shown that the NBC concept may be applied to the blasting of model cylinders and that full scale blasts in the same rock type gives similar results. Thus a set of parallel curves in Figure 18 make a credible proposition. The Swebrec function has asymptotic NBC properties for small fragments when b is constant (Ouchterlony, 2005a). Thus proposition no. 3 gives a physical motivation for this choice and in practice merges with proposition no. 2. Figure 18 shows that the fragmentation curves are basically parallel in the range 0.5-100 mm.

The set of curves in Figure 18 may be called design curves in that they relate any given fraction, e.g. the 0-32 mm road base fraction, to any other fraction, e.g. x_{50}, when the specific charge is changed. The curves predict e.g. that the road base fraction created by blasting will lie between 10 and 20 % when q lies in the range 0.3-0.8 kg/m^3.

DISCUSSION AND CONCLUSION

The procedure to construct the blast design curves for the quarry has the following steps:

- Start with reference rounds, one or preferably several with different values of the specific charge q. Direct sieving or a construction of the complete fragmentation curves from sample piles give reference data for x_{50}, x_{max} and b.
- Based on the reference data, calculate the A-value A' from Equation 3, which corresponds to the measured x50

value (in the Vändle case A' = 3.9). Then a version of Equation 5 may be used to compute the effect on A' of changes in rock mass structure and strength properties.
- Equation 3, with A' instead of A, is then used to compute the effect on x_{50} of a changing q-value. The corresponding x_{max}-data are chosen so that the b-value in Equation 2 is kept constant.
- A set of design curves may now be drawn that could be used to support a first choice of changed blasting pattern.
- If the A-value changes, A' $\rightarrow$ A'new, the original design curves may probably be used anyway, if the q-value for given curve is recalculated as $q_{equiv} = q/(A'/A'_{new})^{1.25}$. Thus if the rock mass becomes easier to blast and $A'_{new} < A'$ then $q_{equiv} < q$, i.e. the specific charge required to obtain a certain fragmentation goes down.
- Alternatively, new design curves for desired q-values may be computed.

In practice there are many ways to change the specific charge, e.g. to change the pattern (burden and spacing), the hole diameter, the bench height, the uncharged part of the blast hole etc. The present procedure is strictly speaking only valid for the first alternative and should de verified by more tests before it is applied to the other alternatives.

The procedures, if not the data could hopefully be transferred to other quarries with other rock and blasting conditions.

The fragmentation model probably has its largest uncertainty for fragments that are close to oversize or x_{max}. Firstly the coarse parts of the constructed fragmentation curves rely on grizzly data and the boulders were not included. Secondly, the number of fragments within a certain size class decreases rapidly with increasing size. , i.e. the statistical description of the fragmentation is expected to become poorer than where there are many fragments in a size class. Thirdly, the Swebrec function approaches the 100 % line at a tangent, which makes the curve fit more sensitive. Fourthly, because of the finite size of any round, the largest boulder represents a finite percentage of the round, i.e. the 100 % point will never be reached in practice.

These observations imply that the fragmentation model probably is less suitable for predicting boulders than the fine fractions. Conversely, samples of fine material from a muck pile contain much useful information about the whole fragmentation curve.

The model has other limitations. Firstly, the design curves show that for a given x50 value it is hardly possible to change the ratio of fine to coarse material in a round, at least by traditional means. In practice short stab holes that fragment the crest layer may do the job though (Chiappetta, 1998).

Further, the effect of the primary crusher has to be considered too. When the feed changes, the amount of crushed road bed fraction e.g. changes too so the ratio of blasted to crushed material in that fraction changes, just as a change of the crusher CSS will alter this ratio.

The fragmentation model above doesn't contain the effect of timing either, which Cunningham's extended Kuz-Ram model does. Onderra, Esen and Jankovic et al. (2004) have developed JKMRC's CZM model (Kanchibotla, Valery & Morrel 1999), in which the amount of material passing a 1 mm mesh is used as a fixed point of the distribution instead of x_{max}. A comparison of the present model with the new one by Onederra et al., more rock mechanics data are needed.

In conclusion, the work presented here utilises the knowledge that the fragment size distribution of blasted rock most likely follows the Swebrec distribution to determine the fragmentation curve of a muck pile from limited information. Once confidence has been gained in this procedure one may perhaps go even further. Some good sieving samples of fine material plus reliable estimates of x_{50} and x_{80} may suffice e.g. Good sieving samples plus estimates of x_{50} and xmax and therefore of b may serve the same purpose.

ACKNOWLEDGEMENTS

Financial support given by the industrial partners in the MinBaS Development Programme, the Swedish Geological Survey, the Swedish Mineral Processing Research Association (MinFo) and the Swedish Energy Administration is gratefully acknowledged. Swerock AB, the owner of the Vändle quarry has supplied in-kind contributions. We are grateful to Swerock's personnel and to Ole and Frederik Smeds of Hallstahammars Sprängtjänst AB who did a really good effort with the drilling job. Lars Granlund and Ingvar Bergquist of Dyno Nobel helped with VOD-measurements and bench profiling. Hiroyuki Arai of the National Police Academy of Japan helped diligently with the field work.

REFERENCES

- Brent, G F and Noy, M J, 2005. Matched pairs blasting technique to quantify the benefits of electronic blasting, in *Proceedings 3rd EFEE World Conference on Explosives and Blasting* (Ed: R Holmberg) pp 481-488 (EFEE: England).
- Chiappetta, R F, 1998. Choosing the right delay timing for the blasting application, optimization and maintaining field control, in *Proceedings 8th High-Tech Seminar on State-of-the Art, Blasting Technology, Instrumentation and Explosives Applications*, (Ed: R F Chiappetta) pp 215-254 (BAI: Allentown PA).
- Cunningham, C V B, 1987. Fragmentation estimations and the Kuz-Ram model – four years on, in *Proceedings 2nd International Symposium on Rock Fragmentation by Blasting*, (Eds: W L Fourney and R D Dick) pp 475-487 (SEM: Bethel CT, USA).
- Cunningham, C V B, 2005. The Kuz-Ram fragmentation model – 20 years on, ? in *Proceedings 3rd EFEE World Conference on Explosives and Blasting* (Ed: R Holmberg) pp 201-210 (EFEE: England).
- Kanchibotla, S S, Valery, W and Morell, S, 1999. Modelling fines in blast fragmentation and its impact on crushing and grinding, in *Proceedings Explo 1999 Conference* (Ed: C Workman-Davies) pp 137-144 (AusIMM: Carlton VIC, Australia).
- Kemeny, J, Girdner, K, Bobo, T and Norton, B, 1999. Improvements for fragmentation measurements by digital imaging: Accurate estimation of fines, in *Proceedings 6th International Symposium on Rock Fragmentation by Blasting* pp 103-109, Symposium series S21 (SAIMM: Johannesburg, South Africa).
- Lilly, P A, 1992. The use of the blastability index in the design of blasts for open pit mines, in *Proceedings of Western Australian Conference of Mining Geomechanics* (Eds: T Szwedzicki, G R Baird and T N Little) pp 421-426 (Curtin Univ Techn, Kalgoorlie WA, Australia).
- Moser, P, Cheimanoff, N, Ortiz, R and Hochholdinger, R, 2000. Breakage characteristics in rock blasting, in *Proceedings 1st EFEE Conference on Explosives & Blasting Technique* (Ed: R Holmberg) pp 165-170 (Balkema: Rotterdam).
- Moser, P, Olsson, M, Ouchterlony, F and Grasedieck, A, 2003. Comparison of the blast fragmentation from lab-scale and full-scale tests at Bårarp, in *Proceedings EFEE 2nd World Conference on Explosives & Blasting*

Technique (Ed: R Holmberg) pp 449-458 (Balkema: Rotterdam).

- Nilsson, N and Perlid, H, 2004. A new system for differentiated charging with gassed bulk emulsion, in *Proceedings of Discussion Meeting BK 2004*, pp 63-74 (Swedish Rock Construction Committee: Stockholm). In Swedish.
- Onederra, I, Esen, S and Jankovic, A, 2004. Estimation of fines generated by blasting - applications for the mining and quarrying industry. *Mining Technology (Transactions of the Institute of Mining and Metallurgy A)* 113:A1-A11.
- Ouchterlony, F, 2005a. The Swebrec function: linking fragmentation by blasting and crushing. *Mining Technology (Transactions of the Institute of Mining and Metallurgy A)* 114:A29-A44.
- Ouchterlony, F, 2005b. What does the fragment size distribution from blasting look like? in *Proceedings 3rd EFEE World Conference on Explosives and Blasting* (Ed: R Holmberg) pp 189-199 (EFEE: England).
- Ouchterlony, F, Olsson, M, Nyberg, U, Potts, G, Andersson, P and Gustavsson, L, 2005. Optimal fragmentation in aggregate quarries, field tests at Vändle. SBMI, Stockholm, MinBaS Rpt 1:11. In Swedish.
- Potts, G, and Ouchterlony, F, 2005. The capacity of image analysis to measure fragmentation, an evaluation using Split DeskTop, Luleå Univ Techn, Sweden, Swebrec Project Rpt.
- Steiner, H J, 1998. Zerkleinerungstechnische Eigenschaften von Gesteinen. *Felsbau* 16:320-325.
- SNRA (2001). ATB Väg 2002. Swedish National Road Authority, Publ no 2001:111.